









Anomalous optical response of graphene on hexagonal boron nitride substrates

Adilet N. Toksumakov ^{1,2,4}, Georgy A. Ermolaev ^{1,3,4}, Mikhail K. Tatmyshevskiy ¹, Yuri A. Klishin¹, Aleksandr S. Slavich¹, Ilya V. Begichev ¹, Dusan Stosic¹, Dmitry I. Yakubovsky¹, Dmitry G. Kvashnin², Andrey A. Vyshnevyy^{1,3}, Aleksey V. Arsenin^{1,3}, Valenty S. Volkov^{1,3}  & Davit A. Ghazaryan ¹ 

Graphene/*h*BN heterostructures can be considered as one of the basic building blocks for the next-generation optoelectronics mostly owing to the record-high electron mobilities. However, currently, the studies of the intrinsic optical properties of graphene are limited to the standard substrates (SiO_2/Si , glass, quartz) despite the growing interest in graphene/*h*BN heterostructures. This can be attributed to a challenging task of the determination of *h*BN's strongly anisotropic dielectric tensor in the total optical response. In this study, we overcome this issue through imaging spectroscopic ellipsometry utilizing simultaneous analysis of *h*BN's optical response with and without graphene monolayers. Our technique allowed us to retrieve the optical constants of graphene from graphene/*h*BN heterostructures in a broad spectral range of 250–950 nm. Our results suggest that graphene's absorption on *h*BN may exceed the one of graphene on SiO_2/Si by about 60%.

¹Center for Photonics and 2D Materials, Moscow Institute of Physics and Technology, Dolgoprudny 141701, Russia. ²Emanuel Institute of Biochemical Physics RAS, Moscow 119334, Russia. ³Emerging Technologies Research Center, XPANCEO, Dubai Investment Park First, Dubai, UAE. ⁴These authors contributed equally: Adilet N. Toksumakov, Georgy A. Ermolaev. email: vsv.mipt@gmail.com; dav280892@gmail.com

Combination of hexagonal boron nitride (*h*BN) with graphene into van der Waals heterostructures attracted much attention at a recent time^{1–4}. *h*BN is an insulator with a large bandgap that possesses a honeycomb crystal structure commensurate to the one of graphene, but with a slight mismatch of the lattice constants. When assembled into such heterostructures in its high-quality single-crystal form, it provides a suppression of external disorder in graphene and an enhancement of electron mobilities. Thus, it has been proven to be a supreme substrate⁵, encapsulating layer^{6,7}, and tunneling barrier^{8,9} in graphene-based electronic devices. Likewise, *h*BN was also found to be an irreplaceable constituent in graphene-based optoelectronic devices, such as photodetectors^{10,11}, DUV electroluminescent devices¹², THz optoelectronic elements^{13,14}, and even light bulbs¹⁵. From the standpoint of optical properties, it is known that the integration of *h*BN with graphene may boost an infrared spectral range absorption when assembled into oriented moiré heterostructures^{16,17}. Several works^{18–20} also report on studies of the total optical response from graphene/*h*BN heterostructures. Nevertheless, the influence of *h*BN substrate or encapsulation on the intrinsic optical response of an almost transparent graphene^{21,22} in the visible spectral range yet remains undetermined.

At the same time, the optical properties of graphene on standard substrates, such as SiO₂/Si, quartz, and a variety of glasses were thoroughly investigated by spectroscopic ellipsometry^{23–29}. Despite the non-identical fitting approaches and graphene samples (exfoliated or chemical vapor deposited), all works agree on the universal value of the absorption, which is defined by the fine-structure constant α . Nonetheless, several works^{16,17,30} argue that this situation may change in the presence of *h*BN.

In this work, we present an experimental investigation of the optical properties of graphene on *h*BN substrates through the imaging spectroscopic ellipsometry technique. We demonstrate an emergence of anomalous optical constants from monolayer graphene on top of a thick *h*BN and compare our results with the ones on one of the standard substrates (SiO₂/Si) from the literature and of our own. We also demonstrate a highly sensitive approach to the detailed analysis of ellipsometric parameters and optical response of graphene, which can potentially be easily extended to other two-dimensional materials.

Results

Before the optical measurements, we confirmed the quality of our exfoliated graphene samples on SiO₂/Si and *h*BN substrates by analyzing their structural properties. Figure 1a, b displays the schematics along with an optical image of one of our samples prepared on SiO₂/Si substrate through standard mechanical exfoliation technique. The acquired Raman spectrum suggests that it is a monolayer with a relative intensity ratio of 2D to G peaks larger than 2 (see inset of Fig. 1b). Figure 1c shows the results of rigorous examination of the surface morphology of our samples by atomic force microscopy (AFM). The roughness histogram of our SiO₂ substrates show a standard deviation of $\sigma_{\text{SiO}_2} \sim 136$ pm for a fitted Gaussian, which is slightly smaller, but in general consistent with the typical values reported elsewhere^{5,31}. On the other hand, in the case of *h*BN substrates, we assemble another set of samples on transparent substrates (glass) through the dry-transfer technique utilizing polycarbonate (PC) films^{32,33}. Figure 1d, e demonstrates the schematics and an optical image of one of the studied heterostructures. The inset of Fig. 1e demonstrates its Raman response proposing a composition of monolayer graphene with a thick *h*BN layer. Performed AFM scans reveal that our samples are free of nanoscale distortions or wrinkles of any kind (see Fig. 1f). A histogram of the

roughness of the *h*BN layer shows a standard deviation of a fitted Gaussian measured to be $\sigma_{h\text{BN}} \sim 37$ pm, which is about three times smaller than for SiO₂ substrates and is also consistent with the typical values reported elsewhere (see inset of Fig. 1f)^{5,31}. A prompt comparison of standard derivations measured for our graphene monolayers on SiO₂ and on *h*BN substrates confirms that those precisely nest on the surfaces of whatever they are placed on (see insets of Fig. 1c, f). Thus, in the case of *h*BN substrates, we obtain ultraflat graphene layers with atomic smoothness.

We used imaging spectroscopic ellipsometry technique to characterize the optical response of our graphene monolayers on both substrates. The schematics of our experimental setup is shown in Fig. 2a. The sensitivity of our technique allows us to study exfoliated and dry-transferred flakes in miniature regions of interest (10 μm^2) within the same field of view³⁴. For both types of substrates, we performed a step-by-step analysis of the optical responses from the samples with and without graphene layers included (see “Methods” for further details). In the case of graphene on *h*BN substrate, the measured and calculated ellipsometric parameters Ψ and Δ are shown in Fig. 2b, c, respectively. Those are in a good agreement as the ones for graphene on SiO₂/Si (see Supplementary Fig. 1).

To obtain the dielectric function of graphene from the acquired ellipsometric spectra, we used the Drude–Lorentz oscillators model (see “Methods”), which considers the optical response of quasi-free electrons (Drude oscillator), and graphene’s van Hove singularity for π -to- π^* interband transitions (Lorentz oscillator)²³.

The determined real $Re[\epsilon]$ and imaginary $Im[\epsilon]$ parts of the dielectric function of graphene on both substrates are shown in Fig. 2d, e, respectively. Unexpectedly, both parts of dielectric function of our ultraflat graphene on *h*BN (sample 1) are noticeably higher than for SiO₂ substrate (sample 2) in the whole interval of measured wavelengths. Additional investigations demonstrate a good repeatability (sample 3). To further validate our findings, we evaluated the transmittance spectrum of graphene/*h*BN heterostructure accounting for the acquired anomalous optical response of graphene and compared it to the measured one. Despite the observed excessive values of graphene’s dielectric function, the theoretical transmittance spectrum matches well with the experimentally observed one as it can be seen in Fig. 2f. In addition, to rule out the possibility that ambiguity of the used optical constants of *h*BN could have caused such an increment in graphene’s optical response, we separately verified the optical response from the thick *h*BN flake using the same micro-transmittance technique (see Supplementary Fig. 2).

In general, the optical responses from atomically thin layers are responsible for a very limited contribution compared to the substrate in the acquired ellipsometric spectra, which causes the accuracy of the measurements to fall. This comes to nearly an extreme case for monolayer graphene.

To enhance the sensitivity of our spectroscopic imaging technique, we assembled a specific configuration of layers giving rise to a larger difference in optical responses from the substrate with and without the graphene layer, and thus, to a higher sensitivity of ellipsometric parameters to graphene optical constants.

This is achieved in the vicinity of topological phase singularities, which arise owing to intersection of graphene optical constant’s dispersion with the substrate zero-reflection surface³⁵. Here, we dry-transferred another graphene/*h*BN heterostructure on top of a thick 200 nm Au film to ensure an appropriate form of a cavity, shown in the schematics and the optical image in Fig. 3a, b, for the realization of topological phase singularity in the vicinity of ellipsometer’s best sensitivity (around ~ 500 nm). The thickness of our *h*BN flake is 152 nm, which leads to a topological

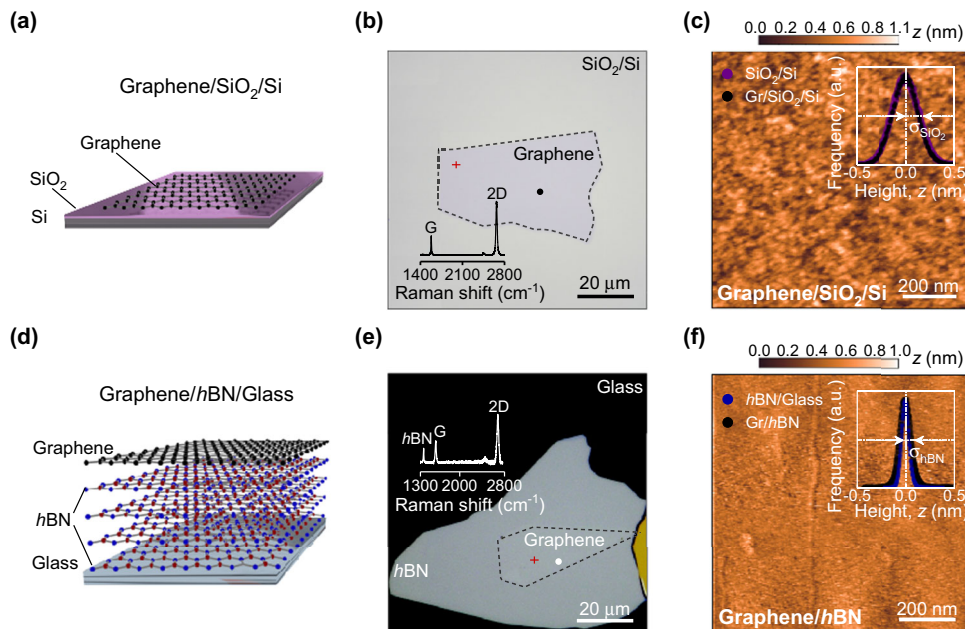


Fig. 1 Surface morphology of monolayer graphene on various substrates. **a** Schematic illustration and **b** $\times 50$ optical image of graphene on SiO_2/Si substrate. Dashed lines are a guide to eye-emphasizing flake boundaries. Inset demonstrates obtained Raman spectrum taken from the point specified by the black dot in **(b)**. **c** Atomic force microscopy (AFM) color map taken from the region specified by the red cross in **(b)**. The color bar shows the surface roughness. Inset shows histograms of the height distribution (surface roughness) for the substrate (SiO_2/Si) and the flake (graphene). **d** Schematic illustration and **e** $\times 50$ optical image of graphene on hBN/glass substrate. Dashed lines are a guide to eye-emphasizing flake boundaries. Inset demonstrates obtained Raman spectrum taken from the point specified by white dot in **(e)**. **f** AFM color map taken from the region specified by the red cross in **(e)**. The color bar shows the surface roughness. Inset shows histograms of the height distribution (surface roughness) for the substrate (hBN/glass) and the flake (graphene).

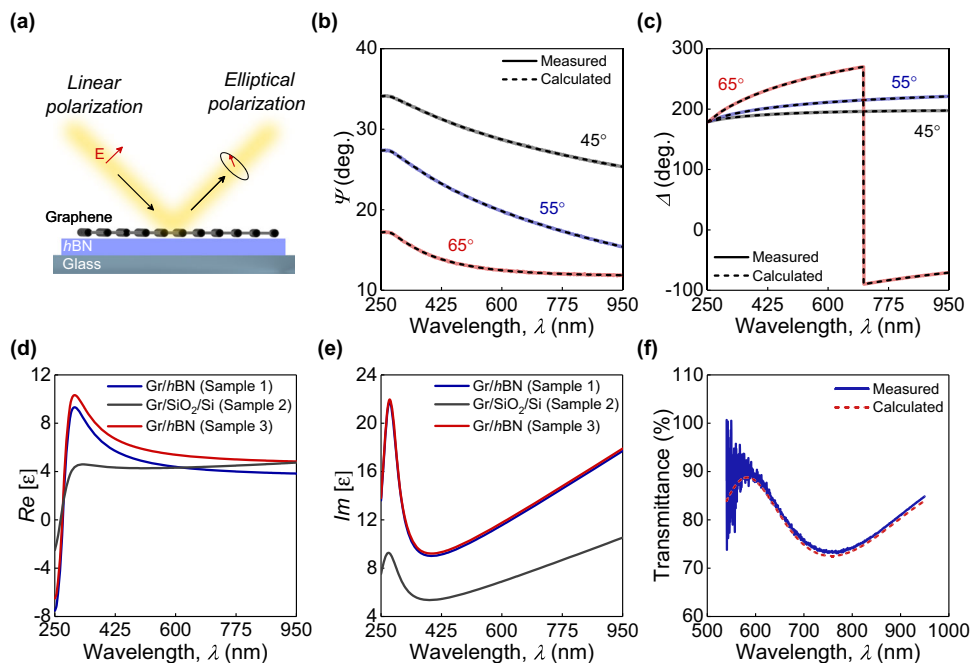


Fig. 2 Imaging spectroscopic ellipsometry of monolayer graphene on hBN/glass substrate. **a** Schematic illustration of the measurement setup. Ellipsometric parameters Ψ **(b)** and Δ **(c)** at three incident angles 45° , 55° , 65° . Solid (dashed) lines represent the measured (evaluated) cases. Real **(d)** and imaginary **(e)** parts of the obtained dielectric function. Gray lines correspond to real and imaginary parts of dielectric function obtained for monolayer graphene on SiO_2/Si substrate. Drude-Lorentz oscillators parameters are collected in Supplementary Table 1. **f** Micro-transmittance spectra of graphene on hBN/glass substrate. Solid (dashed) line represents the measured (evaluated) case.

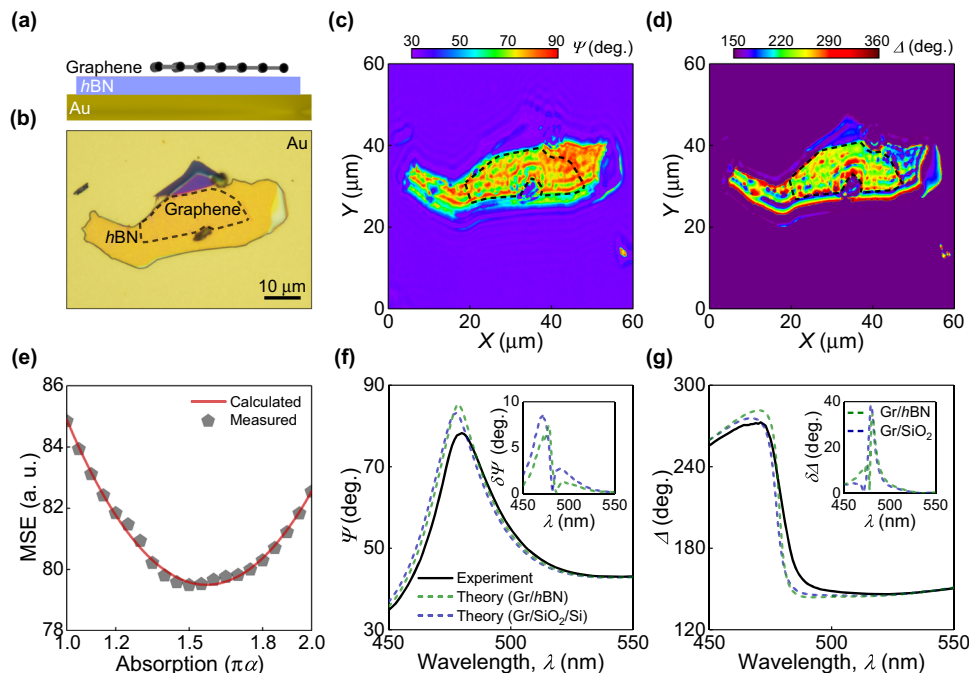


Fig. 3 Highly sensitive optical response to monolayer graphene in the vicinity of topological phase singularity. **a** Schematic illustration and **b** $\times 50$ optical image of graphene on *h*BN/Au substrate. Ellipsometric parameter color maps of Ψ (**c**) and Δ (**d**) at the wavelengths of 477 nm and 50° angle of incidence near the topological phase singularity. The color bars show amplitude (**c**) and phase (**d**) distribution. Dashed lines are a guide to eye-emphasizing flake boundaries. **e** Evaluated (solid line) and measured (gray pentagons) mean squared error (MSE) dependence on the absorbance of graphene. Ellipsometric parameters Ψ (**f**) and Δ (**g**) near the topological phase singularity. Solid lines represent the measured parameters for graphene on *h*BN/Au substrate. Dashed lines correspond to the evaluated parameters. Insets show the exact variation between the evaluated and the measured parameters.

phase singularity at a wavelength of 477 nm. The corresponding ellipsometric parameter maps are presented in Fig. 3c, d.

As expected, Fig. 3d shows a noticeable difference between graphene/*h*BN/Au and *h*BN/Au structures in Δ owing to constructed phase topology. As a result, at this point, we have an increased sensitivity to graphene's optical response. Hence, this allows us to make a unique fit of the optical absorption of our graphene. Here, we calculated the difference between calculated and measured ellipsometry spectra with respect to graphene absorption in terms of mean squared error (MSE). Figure 3e shows the resulting dependence of MSE of our measurements. Surprisingly, it reaches a minimum at values that are larger than $\pi\alpha$, where α is the fine-structure constant^{21,22}, validating our high dielectric permittivity of graphene on *h*BN presented in Fig. 2d, e. This suggests that the typical values of absorption could therefore be mended for our ultraflat graphene on *h*BN substrate.

The corresponding dependences of measured ellipsometric parameters on the wavelength in the vicinity of our topological phase singularity are demonstrated in Fig. 3f, g for Ψ and Δ , respectively. Insets demonstrate the apparent variation between the parameters evaluated for monolayer graphene accounting for two types of substrates studied. Notably, the variation is evidently smaller for the case of a graphene layer placed on an *h*BN substrate.

Figure 4 demonstrates acquired dependencies of refractive indices, extinction coefficients, and the intrinsic absorbance of our exfoliated graphene samples on both types of substrates (SiO_2/Si and *h*BN) in comparison with literature data^{24,26,27} (exfoliated graphene optical constants on a standard SiO_2/Si substrate). Despite the non-identical fitting approaches, all works report on universal optical responses for the case of graphene on SiO_2/Si , including our measurements.

On the other hand, graphene on *h*BN demonstrates substantially higher optical constants (Fig. 4a, b), compared to

graphene on SiO_2/Si . For instance, graphene's refractive index and extinction coefficient is about 20 and 40% higher on *h*BN than on SiO_2/Si , which may be of use for the enhancement of absorption in graphene-based photonic devices^{36,37}. In the case of an excitonic peak at 270 nm, the obtained behavior can be explained by significant difference in static dielectric permittivities of SiO_2 ($\epsilon_{\text{SiO}_2} \sim 3.8$) and *h*BN ($\epsilon_{\text{hBN}} \sim 7$)³⁸, which strongly affects excitonic optical response³⁹. However, the situation in the near-infrared range is more complicated since even high doping of graphene⁴⁰ should not affect its absorption in these spectral intervals (see Supplementary Fig. 3 and Supplementary Note 1).

Nevertheless, angle-resolved photoemission spectroscopy studies³⁰ show that substrates with high dielectric permittivities can substantially modify the fine-structure constants owing to emergence of electron–electron interactions. Indeed, our ab initio calculations suggest that even a slight change in the interlayer distance between graphene and *h*BN may significantly affect the intrinsic optical response (see Supplementary Fig. 4 and Supplementary Note 2). Other approaches also suggest notable growth of optical constants in graphene/van der Waals material heterostructures^{41–44}. Nevertheless, further research is required to explain the physical mechanisms of such an increase in graphene's absorption when placed on top of *h*BN substrate, and other van der Waals materials.

Discussion

Integration of *h*BN and graphene into van der Waals heterostructures results in emergence of extraordinary electronic properties. Therefore, it is of fundamental and practical interest to study the influence of *h*BN on graphene's optical properties. Our imaging spectroscopic ellipsometry measurements showed that *h*BN substrates could substantially enhance the absorption in graphene by $\sim 60\%$ in the broad spectral range (250–950 nm). Hence, those are more suitable than standard SiO_2/Si substrates

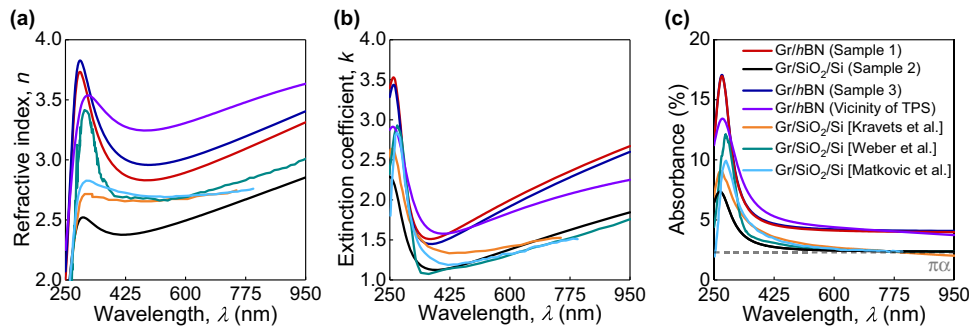


Fig. 4 Comparison of optical constants of exfoliated monolayer graphene on SiO₂/Si and hBN substrates. **a** Refractive indices, **b** extinction coefficients, and **c** intrinsic absorbance A vs wavelength. $A = 4\pi nkt/\lambda$, where n is the refractive index, k is the extinction coefficient, t is the thickness of graphene, and λ is the wavelength of light.

for a variety of photonic applications, where absorption plays a key role, such as photo detection, modulation, and sensing. We attribute this behavior to electron–electron interactions arising due to high static dielectric response of hBN. From a broader perspective, our studies reveal that the universal optical absorption of bare and pristine graphene can be reconstructed in the dielectric environment.

Methods

Sample preparation. We performed O₂ plasma-cleaning for all the types of substrates to enhance the adhesion with two-dimensional layers prior to exfoliation. Next, the substrates were heated up to 120 °C and the standard mechanical exfoliation from bulk graphite and hBN crystals was performed using commercial scotch tapes from “Nitto Denko Corporation”. To integrate graphene monolayers with hBN, we used a polymer-based modified dry-transfer technique^{32,33} established on utilization of double thin films; polydimethylsiloxane (PDMS) and polycarbonate (PC).

Imaging spectroscopic ellipsometry. To analyze the optical constants of graphene samples, we used commercial imaging spectroscopic ellipsometer Accurion nanofilm_ep4 in the nulling operational mode. In our imaging ellipsometer, the spot size is about 2 mm in diameter. The high resolution is achieved not by focusing the light as it is usually done in classical ellipsometers, but by recording the image on a camera as it is shown in Fig. 3c, d. As a result, here, each of the pixels record the ellipsometric parameters, and allow us to take into account only the pixels that correspond to our sample. To avoid backside reflections, we used beam cutter following the approach presented by Funke and colleagues⁴⁵. Ellipsometry spectra were recorded for the spectral range from ultraviolet (250 nm) to near-infrared (950 nm) for the samples on both types of substrates. During the measurements, we simultaneously recorded the ellipsometric signals from bare substrate and substrate with graphene. It allows us to determine the precise optical model of the substrate to eliminate errors arising from slight inconsistencies between literature optical constants and real one for substrate material (Si, SiO₂, glass, and hBN). Note that for the individual ellipsometric parameter analysis of our hBN substrates, we followed the algorithm described in Supplementary Note 2 of our recent work³⁴. Afterward, we fitted graphene optical constants with Drude–Lorentz optical model²³:

$$\varepsilon(E) = \varepsilon_{1\infty} + \varepsilon_{\text{Drude}} + \varepsilon_{\text{Lorentz}} = \varepsilon_{1\infty} - \frac{\hbar^2}{\varepsilon_0 \rho (\tau E^2 + i\hbar E)} + \frac{ABE_0}{E_0^2 - E^2 - iBE} \quad (1)$$

where ε is the dielectric permittivity of graphene, E is the photon energy in eV, $\varepsilon_{1\infty}$ is the offset of the real part of dielectric permittivity, which takes into account absorption peaks for higher than measured energy range, \hbar is the reduced Planck’s constant, ε_0 is the vacuum dielectric constant, ρ is the resistivity in Ω cm, τ is the scattering time in second, A is the Lorentz oscillator strength, B is the Lorentz broadening parameter, and E_0 is the Lorentz peak central energy. In accordance with AFM microscopy results (see Fig. 1c, f), which show negligible roughness, we do not account for the roughness of our samples.

Atomic force microscopy. The morphology of all our samples was examined by AFM (NT-MDT Ntegra II). All measurements were performed in a dry state at room temperature using Hybrid mode. AFM images were acquired using silicon tips (ScanSens, ETALON, HA_NC) with an elastic constant of 3.5 N/m and a resonance frequency of 140 kHz. The areas of 1 μm^2 with 400 pixels per line were obtained at a scanning rate of 0.2 Hz for all samples. The surface height distributions were extracted from areas of 0.2 μm^2 using Gwyddion software.

Data availability

The data that support the plots within this paper and other findings of this study are available from the corresponding authors upon reasonable request.

Received: 27 July 2022; Accepted: 6 January 2023;

Published online: 18 January 2023

References

- Novoselov, K. S. et al. 2D materials and van der Waals heterostructures. *Science* **353**, 6298 (2016).
- Yankowitz, M. et al. Van der Waals heterostructures combining graphene and hexagonal boron nitride. *Nat. Rev. Phys.* **1**, 112–125 (2019).
- Yang, S.-J. et al. Wafer-scale programmed assembly of one-atom-thick crystals. *Nano Lett.* **22**, 1518–1524 (2022).
- Dean, C. et al. Graphene based heterostructures. *Solid State Commun.* **152**, 1275–1282 (2012).
- Dean, C. R. et al. Boron nitride substrates for high-quality graphene electronics. *Nat. Nanotechnol.* **5**, 722–726 (2010).
- Cao, Y. et al. Quality heterostructures from two-dimensional crystals unstable in air by their assembly in inert atmosphere. *Nano Lett.* **15**, 4914–4921 (2015).
- Kretinin, A. V. et al. Electronic properties of graphene encapsulated with different two-dimensional atomic crystals. *Nano Lett.* **14**, 3270–3276 (2014).
- Britnell, L. et al. Field-effect tunneling transistor based on vertical graphene heterostructures. *Science* **335**, 947–950 (2012).
- Mishchenko, A. et al. Twist-controlled resonant tunnelling in graphene/boron nitride/graphene heterostructures. *Nat. Nanotechnol.* **9**, 808–813 (2014).
- Liu, H. et al. High-performance deep ultraviolet photodetectors based on few-layer hexagonal boron nitride. *Nanoscale* **10**, 5559–5565 (2018).
- Viti, L. et al. Thermoelectric graphene photodetectors with sub-nanosecond response times at terahertz frequencies. *Nanophotonics* **10**, 89–98 (2021).
- Song, S.-B. et al. Deep-ultraviolet electroluminescence and photocurrent generation in graphene/hBN/graphene heterostructures. *Nat. Commun.* **12**, 7134 (2021).
- Viti, L. et al. hBN-encapsulated, graphene-based, room-temperature terahertz receivers, with high speed and low noise. *Nano Lett.* **20**, 3169–3177 (2020).
- Bandurin, D. A. et al. Resonant terahertz detection using graphene plasmons. *Nat. Commun.* **9**, 5392 (2018).
- Son, S.-K. et al. Graphene hot-electron light bulb: incandescence from hBN-encapsulated graphene in air. *2D Mater.* **5**, 011006 (2017).
- Abergel, D. S. L. et al. Infrared absorption by graphene–hBN heterostructures. *N. J. Phys.* **15**, 123009 (2013).
- Abergel, D. S. L. et al. Infrared absorption of closely aligned heterostructures of monolayer and bilayer graphene with hexagonal boron nitride. *Phys. Rev. B: Condens. Matter* **92**, 115430 (2015).
- Jia, Y. et al. Tunable plasmon–phonon polaritons in layered graphene–hexagonal boron nitride heterostructures. *ACS Photonics* **2**, 907–912 (2015).
- Ni, G. X. et al. Fundamental limits to graphene plasmonics. *Nature* **557**, 530–533 (2018).
- Rigosi, A. F. et al. Measuring the dielectric and optical response of millimeter-scale amorphous and hexagonal boron nitride films grown on epitaxial graphene. *2D Mater.* **5**, 011011 (2018).
- Katsnelson, M. I. *Graphene: Carbon in Two Dimensions* (Cambridge University Press, 2012).
- Nair, R. R. et al. Fine structure constant defines visual transparency of graphene. *Science* **320**, 1308 (2008).

23. El-Sayed, M. A. et al. Optical constants of chemical vapor deposited graphene for photonic applications. *Nanomaterials* **11**, 1230 (2021).
24. Kravets, V. G. et al. Spectroscopic ellipsometry of graphene and an exciton-shifted van Hove peak in absorption. *Phys. Rev. B: Condens. Matter* **81**, 155413 (2010).
25. Matković, A. et al. Influence of transfer residue on the optical properties of chemical vapor deposited graphene investigated through spectroscopic ellipsometry. *J. Appl. Phys.* **114**, 093505 (2013).
26. Matković, A. et al. Spectroscopic imaging ellipsometry and Fano resonance modeling of graphene. *J. Appl. Phys.* **112**, 123523 (2012).
27. Weber, J. W. et al. Optical constants of graphene measured by spectroscopic ellipsometry. *Appl. Phys. Lett.* **97**, 091904 (2010).
28. Nelson, F. J. et al. Optical properties of large-area polycrystalline chemical vapor deposited graphene by spectroscopic ellipsometry. *Appl. Phys. Lett.* **97**, 253110 (2010).
29. Ochoa-Martínez, E. et al. Determination of a refractive index and an extinction coefficient of standard production of CVD-graphene. *Nanoscale* **7**, 1491–1500 (2015).
30. Hwang, C. et al. Fermi velocity engineering in graphene by substrate modification. *Sci. Rep.* **2**, 590 (2012).
31. Rokni, H. et al. Direct measurements of interfacial adhesion in 2D materials and van der Waals heterostructures in ambient air. *Nat. Commun.* **11**, 5607 (2020).
32. Zomer, P. J. et al. Fast pick up technique for high quality heterostructures of bilayer graphene and hexagonal boron nitride. *Appl. Phys. Lett.* **105**, 013101 (2014).
33. Son, S. et al. Strongly adhesive dry transfer technique for van der Waals heterostructure. *2D Mater.* **7**, 041005 (2020).
34. Ermolaev, G. A. et al. Giant optical anisotropy in transition metal dichalcogenides for next-generation photonics. *Nat. Commun.* **12**, 854 (2021).
35. Ermolaev, G. et al. Topological phase singularities in atomically thin high-refractive-index materials. *Nat. Commun.* **13**, 2049 (2022).
36. Yao, Y. et al. Broad electrical tuning of graphene-loaded plasmonic antennas. *Nano Lett.* **13**, 1257–1264 (2013).
37. Kananen, T. et al. Graphene absorption enhanced by quasi-bound-state-in-continuum in long-wavelength plasmonic–photonic system. *Adv. Optical Mater.* **10**, 2201193 (2022).
38. Laturia, A. et al. Dielectric properties of hexagonal boron nitride and transition metal dichalcogenides: from monolayer to bulk. *npj 2D Mater. Appl.* **2**, 6 (2018).
39. Raja, A. et al. Coulomb engineering of the bandgap and excitons in two-dimensional materials. *Nat. Commun.* **8**, 15251 (2017).
40. Ma, Q. et al. Tunable optical properties of 2D materials and their applications. *Adv. Optical Mater.* **9**, 2001313 (2021).
41. Qiu, B. et al. Optical properties of graphene/MoS₂ heterostructure: first principles calculations. *Nanomaterials* **8**, 962 (2018).
42. Ma, Y. et al. Optical parameters of graphene/MoS₂ van der Waals heterostructure investigated by spectroscopic ellipsometry. *Appl. Surf. Sci.* **599**, 153987 (2022).
43. Pham, K. D. et al. Two-dimensional van der Waals graphene/transition metal nitride heterostructures as promising high-performance nanodevices. *N. J. Chem.* **45**, 5509–5516 (2021).
44. Ma, Y. et al. Chemical vapor deposition of two-dimensional molybdenum nitride/graphene van der Waals heterostructure with enhanced electrocatalytic hydrogen evolution performance. *Appl. Surf. Sci.* **589**, 152934 (2022).
45. Funke, S. et al. Imaging spectroscopic ellipsometry of MoS₂. *J. Phys. Condens. Matter* **28**, 385301 (2016).

Acknowledgements

This work was supported by Russian Science Foundation project No. 21-79-00218 and Ministry of Science and Higher Education of the Russian Federation Agreement No. 075-15-2022-1150 (topological phase singularity studies). The ab initio calculations were performed using resources provided by the Joint Supercomputer Center of the Russian Academy of Sciences.

Author contributions

V.S.V. and D.A.G. suggested and directed the project with the help from A.V.A. A.N.T., Yu.A.K., I.V.B., and D.A.G. fabricated the samples, G.A.E., M.K.T., A.S.S., D.S., and D.I.Y. performed the measurements and analyzed the data, A.N.T., D.G.K., and A.A.V. provided theoretical support. A.N.T., G.A.E., A.A.V., A.V.A., V.S.V., and D.A.G. contributed to the interpretation of the experimental results. A.N.T. and G.A.E. prepared the figures and wrote the original draft. A.A.V., A.V.A., V.S.V., and D.A.G. reviewed and edited the paper. All authors contributed to the discussions and commented on the paper.

Competing interests

The authors declare no competing interests.

Additional information


Supplementary information The online version contains supplementary material available at <https://doi.org/10.1038/s42005-023-01129-9>.

Correspondence and requests for materials should be addressed to Valentyn S. Volkov or Davit A. Ghazaryan.

Peer review information *Communications Physics* thanks the anonymous reviewers for their contribution to the peer review of this work.

Reprints and permission information is available at <http://www.nature.com/reprints>

Publisher's note Springer Nature remains neutral with regard to jurisdictional claims in published maps and institutional affiliations.

 **Open Access** This article is licensed under a Creative Commons Attribution 4.0 International License, which permits use, sharing, adaptation, distribution and reproduction in any medium or format, as long as you give appropriate credit to the original author(s) and the source, provide a link to the Creative Commons license, and indicate if changes were made. The images or other third party material in this article are included in the article's Creative Commons license, unless indicated otherwise in a credit line to the material. If material is not included in the article's Creative Commons license and your intended use is not permitted by statutory regulation or exceeds the permitted use, you will need to obtain permission directly from the copyright holder. To view a copy of this license, visit <http://creativecommons.org/licenses/by/4.0/>.

© The Author(s) 2023